

Hydrodynamics of evaporating sessile drops

L.Yu. Barash, L.N. Shchur

Landau Institute for Theoretical Physics, 142432 Chernogolovka, Russia

Abstract

Several dynamical stages of the Marangoni convection of an evaporating sessile drop are obtained. We jointly take into account the hydrodynamics of an evaporating sessile drop, effects of the thermal conduction in the drop and the diffusion of vapor in air. The stages are characterized by different number of vortices in the drop and the spatial location of vortices. During the early stage the array of vortices arises near a surface of the drop and induces a non-monotonic spatial distribution of the temperature over the drop surface. The number of near-surface vortices in the drop is controlled by the Marangoni cell size, which is calculated similar to that given by Pearson for flat fluid layers. The number of vortices quickly decreases with time, resulting in three bulk vortices in the intermediate stage. The vortex structure finally evolves into the single convection vortex in the drop, existing during about 1/2 of the evaporation time.

1. Introduction

Evaporation of a drop in an ambient gas was considered since Maxwell time mainly as diffusion of vapor from a near-surface layer [1, 2, 3]. Classical quasistationary theory of evaporation of a drop does not include effects of fluid dynamics in the drop and only partially takes into account basic effects of heat transfer. Recently a number of new applications has stimulated much attention to the problem again. This is associated, for example, with preparing ultra-clean surfaces [4, 5, 6, 7], protein crystallography [8, 9], the studies of DNA stretching behavior and DNA mapping methods [10, 11, 12], developing methods for jet ink printing [13, 14, 15], and with other fields (see, for example, [16]). Of particular interest is the process of evaporation of the drop containing the colloidal suspension [17, 18, 19]. One of typical experimental situations is an observation of an evaporating drop lying on a substrate, where the contact line of the drop is pinned to the edge of the substrate. Ordered structures of nanoparticles can arise on the drop surface during the evaporation process. After the drop dries out the ordered structures are left also on the substrate. An important example is the self-assembly of long-range-ordered nanocrystal superlattice monolayer [17, 18, 19].

Other example, where depinning of the contact line is revealed, is the effect of evaporative contact line deposition, the so-called coffee-ring effect [20, 21, 22, 23, 24, 25]. These aspects altogether resulted in the interest to the problem and respective significant activity of experimentalists and theorists during the past decade.

For theoretical description of problems mentioned above, the classical theory of drop evaporation, which was used up to recent years, turned out to be insufficient, too simplified and not including a number of important processes. For example, role of pinned contact line during the evaporation process, and fluid dynamics effects within the evaporating drops of capillary size, were analysed and new important aspects were found. As a result, a development in experimental studies and progress in understanding of evaporation process have been achieved during past decade [20, 21, 24, 26, 27, 28, 29].

It was found, in particular, that the evaporating flux density is inhomogeneous along the surface and has an integrated singularity on approach to the pinned contact line [20, 21]. The resulting inhomogeneous mass flow can strongly modify the temperature distribution over the drop surface and, hence, the Marangoni forces associated with the temperature dependent surface tension. The convection inside a droplet [27, 28, 30, 31, 32, 33, 34, 35, 36, 37,

Email address: barash@itp.ac.ru (L.Yu. Barash)

38, 39, 40, 41] appears to be quite different from the classical Marangoni convection in the systems with a simple flat geometry [42, 43]. Thermal conductivity of the substrate can also influence the formation of flows within a liquid drop since it is the magnitude of the conductivity which determines the sign of the tangential component of the temperature gradient at the surface close to the contact line and, therefore, the direction of the convection [29].

The observation of the distinct stages of the evaporation process [44, 45, 46] has revealed that the longest and dominating regime of the evaporation process is the constant contact area mode, where the contact line is pinned. On a later stage the contact line gets depinned and the different regime, the constant contact angle mode switches on. Finally, the drying mode follows, in which the height, the contact area and the contact angle rapidly decrease with time.

Recently, evolved numerical calculations have been carried out for providing simultaneous descriptions of the fluid dynamics, the vapor diffusion and the spatial temperature distribution in an axially symmetrical evaporating sessile drop. The corresponding quasistationary problem was studied in [27, 28]. The dynamical description of the liquid drop evaporation was developed in [47]. Taking into account quantitatively the important components of the evaporation process, we have obtained, in particular, the time evolution of the temperature and the fluid convection in the drop.

2. Dynamics of vortex structure

Our calculations demonstrate the presence of several characteristic stages of the thermocapillary convection. During the early regime of the dynamics of the Marangoni convection, for various liquids and drop sizes, the vortices arise near the surface of the drop. For the toluene drop, this regime quickly arises and evolves up to $t \approx 0.3$ s. This is quite a short time period for the toluene drop as compared with the total evaporation time ≈ 550 s, but it admits an experimental study. The vortices grow, the number of vortices decreases, and eventually they evolve into the bulk of the drop. This can be seen in Fig. 1 where the vortex structure contains four pairs of near-surface vortices and a corner vortex, and the temperature displays just four humps at the surface. This number of vortices in the drop is controlled by the Marangoni cell size, which is calculated similar to that given by Pearson for flat

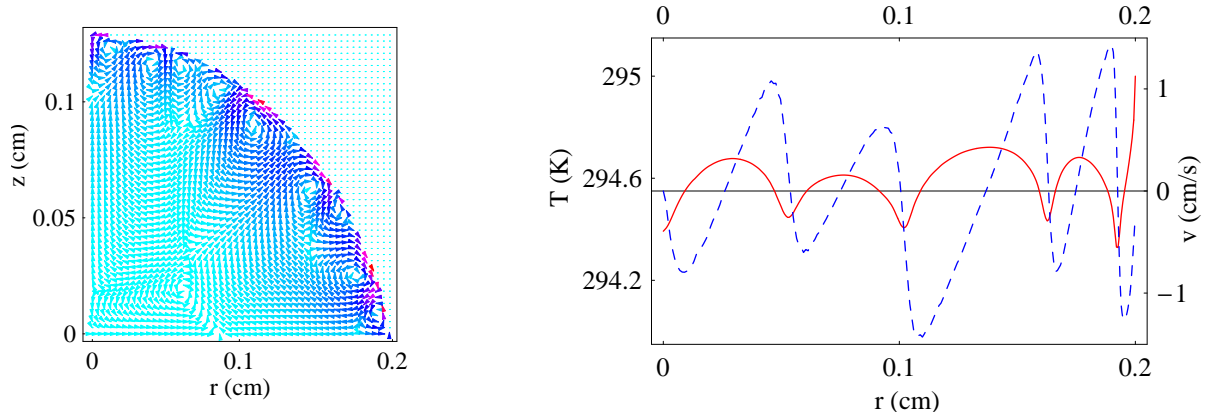
fluid layers. The existence of near-surface vortices and the associated humps in the profile of the surface temperature, become more pronounced with the decrease of the viscosity of the liquid. There are no near-surface vortices when the viscosity increases more than in four times as compared with the toluene drop. Near-surface vortices were observed experimentally in studying evaporating sessile drops of FC-72 on a copper substrate [30, 31].

As seen in Fig. 1, the extrema of the surface temperature correspond to the change of sign of the tangential component of velocities at the surface. The reason for this behavior is that the fluid flow moves from the higher to the lower temperature regions of the surface, because the surface tension decreases with increasing the temperature. The flows result in a redistribution of the temperature due to the convective heat transfer. The number of the surface temperature humps and the number of the near-surface vortices decrease during their evolution.

If the thermal conductivity of a substrate is large compared to that of the liquid, then the temperature can be maintained practically constant at the substrate-fluid interface. This is the case, in particular, for the silicon nitride substrates used in experiments [17, 18, 19]. The silicon nitride is a material with high thermal conductivity, approximately in three orders larger than for the toluene. For this reason, the boundary condition for the temperature distribution at the substrate can be reduced to the constant temperature. Heat transfer between the substrate and the drop plays an important role in establishing the temperature profile in the drop. High substrate conductivity also excludes a possibility for the reversal of the Marangoni flows [29], taking place for substrates with relatively small thermal conductivity.

The initial conditions chosen when generating Fig. 1 were: zero velocity values, constant room temperature, and absence of vapor. For a description of a real experiment they have to be slightly modified to include the weak stochastic distribution of the surface temperature and velocities. We have carried out such calculations using a small-scale stochastic initial conditions. This has changed the particular behavior of the fluid dynamics only on the initial stage of the process, where a large number of small-scale surface vortices arise. Then the surface vortex structure quickly evolves into exactly the same one as we obtained for the basic initial conditions. This result demonstrates the

Figure 1: (Color online.) Left panel: The velocity field at $t = 0.16$ s. Right panel: Temperature (solid line) and velocity (dashed line) along the drop surface as functions of the radius at $t = 0.16$ s. The velocity changes its sign at crossing points with the horizontal axis.



generic character of the near-surface vortex regime in Fig. 1 at the early stage of the formation of the Marangoni convection.

An initial velocity field within the sessile drop can also be strongly disturbed right after the drop has fallen down on the substrate, or for some other reason. We model such a situation by choosing random initial conditions for the bulk velocity field, which are in agreement with the continuity equation for the incompressible fluid. We find that strong disturbances of the bulk velocities can noticeably modify the initial stage of the drop dynamics, but they do not modify its main stage. For the initial random velocities of the order of 5 cm/s (which well exceeds the typical velocity in the vortex 1 cm/s), the difference between the dynamics of the disturbed and resting drops disappears after $t \approx 0.5$ s. This verifies the stability of the large-scale drop dynamics with respect to disturbances of the initial temperature and velocity fields.

During the enlargement of the near-surface vortices, their number decreases, and the convection involves the bulk of the drop. As a result, for $t \approx 0.45$ s, three bulk vortices control the velocity and temperature fields in the drop, as seen in left panels in Figs. 2,3. During the coexistence of three vortices, the corner vortex starts growing at the expense of the other two vortices, and eventually at $t \approx 2.0$ s it occupies the whole drop volume. A spatial dependence of the temperature along the drop surface is nonmonotonic, if the drop contains more than one vortex (see Fig. 3). Right panels in Figs. 2,3 demonstrate how in the single-vortex regime effects of Marangoni forces drive liquid along

the surface to the apex, where the fluid penetrates along the symmetry axis in the depth of the drop.

The regime with the single vortex represents one of the main stages of the dynamics of the evaporating sessile drop. It lasts up to $t \approx 250$ s. More than half of the drop mass evaporates during this period of time. If the initial values of mass, height and contact angle of the drop are $m = 8.7$ mg, $h = 0.1314$ cm, $\theta = 1.2045$, then at the moment $t = 250$ s we find $m = 4.0$ mg, $h = 0.0685$ cm, $\theta = 0.716$. In particular, $h/(2r_0) \approx 0.17$, i.e. the drop shape is noticeably flattened. We remind that the total time of the evaporation of the toluene drop is 508 s.

The quasistationary single-vortex state loses its stability at $t \approx 250$ s and the vortex acquires a pronounced nonstationary character. During this nonstationary regime, the fluid pulsations take place. The characteristic frequency of the pulsations corresponds to the circulation period 0.15 s of a fluid element in the original vortex. Initially the pulsations are concentrated near the center of the original vortex. Then, the single-cell pulsating state breaks into two-center (and later three-center) pulsating structure (see Fig. 10 in [47]). Eventually at $t \approx 300$ s a quasistationary state with three vortices arises.

The numerical calculations of the fluid dynamics were tested with several different mesh sizes. The respective results are qualitatively identical and show reliable convergence of the quantitative characteristics. For example, the single-vortex regime was found to arise at 3.48 s, 2.48 s, 2.2 s, 2.06 s, 2.01 s for 100×100 , 150×150 , 200×200 , 250×250 ,

Figure 2: (Color online.) Left panel: The velocity distribution at $t = 0.5$ s. The stage of drop dynamics with three vortices takes place from $t \approx 0.45$ s to $t \approx 2.0$ s. Right panel: The velocity distribution at $t = 30$ s. A distribution with a single vortex takes place from $t \approx 2.0$ s to $t \approx 250$ s.

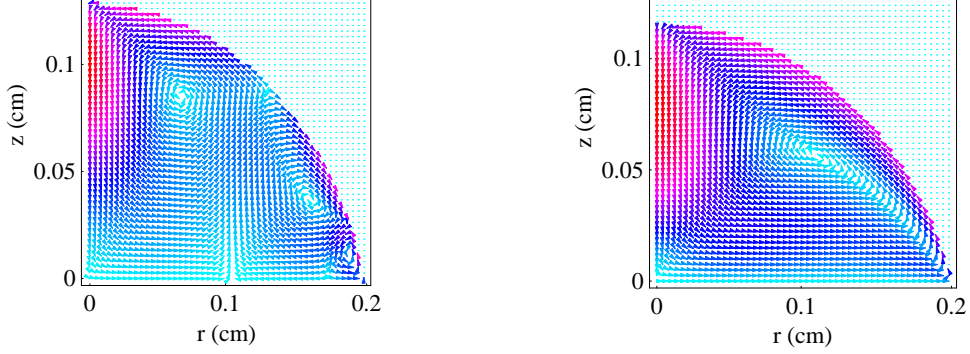
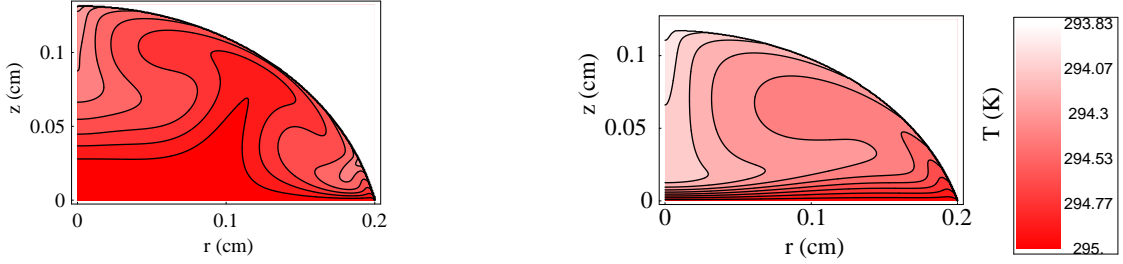


Figure 3: (Color online.) Distributions of temperature within drop for the stages of drop dynamics with three vortices (left) and a single vortex (right). The distributions are taken at $t = 0.5$ s and at $t = 30$ s correspondingly. Temperature scale shown at the right column.



300×300 mesh elements covering a half of the drop cross-section.

3. Numerical method

The simultaneous calculation of the physical quantities in the drop can be partitioned into several steps:

1. We apply to the diffusion equation $\partial u / \partial t = D \Delta u$ the implicit finite difference method using irregular mesh outside the drop and a variable time step. We use a boundary interpolation in a vicinity of the drop surface [47]. For the boundary conditions we take $u = u_s$ on the drop surface, $u = 0$ far away from the drop, $\partial u / \partial r = 0$ and $\partial u / \partial z = 0$ on the axes $r = 0$ and $z = 0$ correspondingly.

In order to calculate accurately the vapor density in quite a large region, it is convenient to use irregular mesh. We use the mesh with sufficiently small steps near the drop surface and with exponentially increasing steps, which are

chosen in accordance with the decay of the vapor density, which can be estimated analytically.

2. Calculations of the stream function ψ and velocities \mathbf{v} inside the drop are based on Eq. $\partial^2 \psi / \partial r^2 - \partial \psi / r \partial r + \partial^2 \psi / \partial z^2 = r \gamma$, where γ is vorticity. The implicit finite difference method with a regular mesh inside the drop is applied. We use a boundary interpolation near the drop surface. For the boundary conditions we take $\psi = 0$ at all boundaries: on the surface of the drop and on the axes $r = 0$ and $z = 0$.
3. We solve Eq. $\partial \gamma(r, z) / \partial t + (\mathbf{v} \cdot \nabla) \gamma(r, z) = \nu (\Delta \gamma(r, z) - \gamma(r, z) / r^2)$ to obtain the vorticity γ inside the drop. The explicit finite difference method with a regular mesh inside the drop is used. We use a boundary interpolation close to the drop surface. For the boundary conditions we take $\gamma = 0$ for $r = 0$; $\gamma = \partial v_r / \partial z$ for $z = 0$; $\gamma = d\sigma / (\eta ds) + 2v_r d\phi / ds$ on the drop surface, where $d\sigma / ds = -\sigma' \partial T / \partial s$ is the derivative of the surface tension along the drop surface.

4. For calculating the temperature T inside the drop, the explicit finite difference method with a regular mesh is applied to the thermal conduction equation $\partial T/\partial t + \mathbf{v} \cdot \nabla T = \kappa \Delta T$. We use a boundary interpolation in a vicinity of the drop surface. The boundary conditions take the form $\partial T/\partial r = 0$ for $r = 0$; $T = T_0$ for $z = 0$; $\partial T/\partial n = -Q_0(r)/k = -LJ(r)/k$ on the drop surface. Here $Q_0(r)$ is the rate of heat loss per unit area of the free surface, \mathbf{n} is a normal vector to the drop surface.
5. During the iterative procedure, the drop shape is recalculated in accordance with the evaporative mass loss for the respective time interval. This is possible due to a quasistationary character of the shape change of the drop. Deviations of a drop profile from a spherical cap are taken into account [47, 48].

4. Discussion

We have developed the approach for studying the evaporation and fluid dynamics of a sessile drop of a capillary size and applied it for the description of the toluene drop evaporation. In particular, the approach allows to obtain the time evolution of vortex structure and temperature distribution in evaporating sessile drops. The appearance of near-surface vortices on the early stage of the evaporation process of sessile drops is predicted. We also obtained three bulk vortices in the intermediate stage. They finally evolve into the single convection vortex in the drop, existing during about 1/2 of the evaporation time. Possible development of the method include description of hydrodynamics of colloidal drops, and study of influence of substrate conductivity on the dynamics of vortex structure.

References

- [1] J.C. Maxwell, *Diffusion*, collected scientific papers, Encyclopedia Britannica, Cambridge, 1877.
- [2] I. Langmuir, Phys. Rev. **12**, 368 (1918).
- [3] N. A. Fuchs, *Evaporation and droplet growth in gaseous media* (Pergamon Press, Oxford, 1959).
- [4] A. F. Leenaars, J. A. M. Huethorst, J. J. van Oekel, Langmuir **6**, 1701 (1990).
- [5] J. Marra, J. A. M. Huethorst, Langmuir **7**, 2748 (1991).
- [6] J. A. M. Huethorst, J. Marra, Langmuir **7**, 2756 (1991).
- [7] O. K. Matar, R. V. Craster, Phys. Fluids **13**, 1869 (2001).
- [8] N. D. Denkov et. al., Langmuir **8**, 3183 (1992).
- [9] A. S. Dimitrov et. al., Langmuir **10**, 432 (1994).
- [10] J. P. Jing et. al., Proc. Natl. Acad. Sci. U.S.A. **95**, 8046 (1998).
- [11] M. Chopra, L. Li et. al., J. of Rheology **47**, 1111 (2003).
- [12] C. Hsieh, L. Li, R. G. Larson, J. Non-Newtonian Fluid Mech **113**, 147 (2003).
- [13] J. Park, J. Moon, Langmuir **22**, 3506 (2006).
- [14] J. Jong et. al., Appl. Phys. Lett. **91**, 204102 (2007).
- [15] J. Lim et. al., Adv. Funct. Mater. **18**, 229 (2008).
- [16] A. Frohn and N. Roth, *Dynamics of Droplets* (Berlin, Springer, 2000).
- [17] X. M. Lin, H. M. Jaeger, C. M. Sorensen, K. J. Klabunde, J. Phys. Chem., B **105**, 3353 (2001).
- [18] S. Narayanan, J. Wang, X. M. Lin, Phys. Rev. Lett. **93**, 135503 (2004).
- [19] T. P. Bigioni, X. M. Lin, T. T. Nguyen, E. I. Corwin, T. A. Witten, H. M. Jaeger, Nature Materials **5**, 265 (2006).
- [20] R. D. Deegan et al., Nature **389**, 827 (1997).
- [21] R. D. Deegan et al., Phys. Rev. E **62**, 756 (2000).
- [22] L. V. Govor, G. Reiter, J. Parisi, G. H. Bauer, Phys. Rev. E **69**, 061609 (2004).
- [23] H. Hu, R. G. Larson, J. Phys. Chem. B, **110**, 7090 (2006).
- [24] Y. O. Popov and T. A. Witten, Phys. Rev. E **68**, 036306 (2003).
- [25] R. Zheng, Y. O. Popov, T. A. Witten, Phys. Rev. E **72**, 046303 (2005).
- [26] H. Hu, R. G. Larson, J. Phys. Chem. B **106**, 1334 (2002).
- [27] H. Hu, R. G. Larson, Langmuir **21**, 3972 (2005).
- [28] F. Girard, M. Antoni, S. Faure, A. Steinchen, Langmuir **22**, 11085 (2006).
- [29] W. D. Ristenpart, P. G. Kim, C. Domingues, J. Wan, H. A. Stone, Phys. Rev. Lett. **99**, 234502 (2007).
- [30] K. Sefiane, J. R. Moffat, O. K. Matar, R. V. Craster, Appl. Phys. Lett. **93**, 074103 (2008).
- [31] K. Sefiane, A. Steinchen, R. Moffat, Colloids Surf. A **365**, 95–108 (2010).
- [32] N. L. Zhang, W. J. Yang, Trans. ASME **104**, 656 (1992).
- [33] S. H. Davis, J. Fluid Mech. **39**, 347 (1969).
- [34] P. Ehrhard, S. H. Davis, J. Fluid Mech. **229**, 365 (1991).
- [35] D. M. Anderson, S. H. Davis, Phys. Fluids **7**, 248 (1995).
- [36] A. Oron, S. H. Davis, S. G. Bankoff, Rev. Mod. Phys. **69**, 931 (1997).
- [37] D. Lozinski, M. Matalon, Physics of Fluids A **5**, 1596 (1993).
- [38] B. D. Niazmand, H. A. Shaw, H. A. Dwyer, I. Aharaon, Combustion Sci. Technol. **103**, 219 (1995).
- [39] A. Ye. Rednikov, V. N. Kourdiumov, Yu. S. Ryazantsev, M. G. Velarde, Phys. Fluids **7**, 2670 (1995).
- [40] R. Savino, D. Paterna, N. Favaloro, J. Thermophys. Heat Transfer **16**, 562 (2002).
- [41] X. Xu, J. Luo, Appl. Phys. Lett. **91**, 124102 (2007).
- [42] H. Benard, Rev. Gen. Sci. Pures Appl. **11**, 1261 (1900).
- [43] J. R. A. Pearson, J. Fluid Mech. **4**, 489 (1958).
- [44] R. G. Picknett, R. J. Bexon, J. Colloid Interface Sci. **61**, 336 (1977).
- [45] M. E. R. Shanahan, C. Bourges, Int. J. Adhes. Adhes. **14**, 201 (1994).
- [46] C. Bourges, M. E. R. Shanahan, Langmuir **11**, 2820 (1995).
- [47] L. Yu. Barash, T.P. Bigioni, V.M. Vinokur, and L.N. Shchur, Phys. Rev. E **79**, 046301 (2009).
- [48] L. Yu. Barash, Phys. Rev. E **79**, 025302(R) (2009).